Astron. Astrophys. 351, 373–381 (1999)

ASTRONOMY AND ASTROPHYSICS

Analysis of coronal emissions observed at meter wavelengths

P. Lantos[1] **and C.E. Alissandrakis**[2]

[1] Observatoire de Paris-Meudon, 92195 Meudon, France
[2] Section of Astrogeophysics, University of Ioannina, 45110 Ioannina, Greece

Received 18 February 1999 / Accepted 26 August 1999

Abstract. We present an extensive analysis of large and medium scale radio sources observed with the Nançay Radioheliograph at 169 MHz, over more than four solar rotations in 1984 (during the declining phase of the solar cycle). The large scale emission is dominated by the coronal plateau, the radio counterpart of the coronal plasma sheet, which had an oscillatory structure around the equator. Medium scale local sources include both faint noise storm continua and thermal sources. Noise storm continua have greater brightness ($8\,10^5$ to $3.8\,10^6$ K) and smaller diameter than thermal sources. We present distributions of brightness temperatures, sizes as well as longitude and latitude of the thermal sources and we study their location with respect to faculae and neutral lines. Based on their rotation rate, we estimate their altitude at 70 000 km. We find that most thermal sources at 169 MHz are located between faculae and neutral lines and we present a geometrical model to account for this observation, according to which these sources are located in the upper leg of large scale loops. A small number of thermal sources is closer to neutral lines; these might be loops at the base of isolated coronal streamers.

Key words: Sun: corona – Sun: radio radiation

1. Introduction

After the launch of satellites extending the range of coronal observations to X-ray and EUV wavelengths, there has been a renewal of interest in the quiet sun. Observations of the sun at radio wavelengths provide means to map the corona on the solar disk at different altitudes, depending upon the frequency used. At long-decimeter wavelengths, the radio maps are globally similar to the X-ray observations, but, because they are sensitive to lower densities, longer wavelengths give a quite different view, in particular with respect to the emission sources (see review by Lantos, 1999). In the decameter range the source emissions are frequently related to helmets of coronal streamers (see for example Schmahl et al., 1994) while in the metric range emissions come from loops at lower altitudes and thus the brightness distribution is again very different.

Send offprint requests to: P. Lantos

Quiet sun observations at meter wavelengths have been made on a regular basis with the Nançay Radioheliograph since 1980 using aperture synthesis methods. It has been shown that the nature of the emission sources is changing with the solar cycle: faint noise storm continua are very frequent during the maximum on the cycle (Alissandrakis et al., 1985) while, during the minimum, emission sources are due to denser loop systems, even when there is no active region on the solar disk (Lantos et al., 1992). During intermediate periods, like the period studied here (two years before minimum), different kinds of emission sources coexist. This period, covering more than four Carrington rotations (in spring and summer 1984), was relatively quiet. During two of the Carrington rotations, only a few days were missing because strong noise storms prevent computations of 2-dimensional maps.

A further reason for interest in the 1984 period is that a number of complementary data were available at that time: synoptic maps of the K-corona, of the emission line corona, of the photospheric magnetic field and its extrapolation. Chromospheric synoptic charts from NOAA-Boulder are no longer available and those from Meudon Observatory are not available for recent years. Thus the period of 1984 has been studied using radio synoptic maps by Alissandrakis & Lantos (1996, hereafter referred to as paper I) who compared radio observations with chromosphere structures and with the photospheric magnetic field, and by Lantos & Alissandrakis (1996, hereafter referred to as paper II), for the comparison with the optical corona. Using a statistical method appropriate in the case where the sample of sources is limited, it was shown in particular in paper I that radio sources observed at meter wavelengths were closely related to neutral lines of the photospheric magnetic field, but in general not located above the neutral line. One of the purposes of the present work, which is based on daily maps, is to identify more precisely the nature of those sources which, during this period of the solar cycle, appear to be the most frequent. We are analysing here the maps to derive further characteristics of the large and medium-scale structures of the corona.

2. Observations and data reduction

The observations were obtained with the Nançay radioheliograph at 169 MHz (λ = 1.77 m). At that time the instrument

consisted of two independent arrays, one in the East-West and the other in the North-South direction. Each array operated as a fan beam synthesis instrument, normally at a rate of 25 images per second (Radioheliograph Group, 1983).

The East-West array consisted of 16 antennas of 3 m diameter and 2 antennas of 10 m diameter. Each large antenna was correlated with each small, resulting in 32 two-element interferometers with baselines from 100 to 3200 m (56 to 1800 wavelengths) in steps of 100 m. The North-South array consisted of 11 antennas of 5 m diameter; each antenna was correlated with the central antenna of the East-West array, forming 11 two-element interferometers with baselines from 109 to 1195 m (61 to 670 wavelengths). The spatial resolution is $1.15'$ in the east-west direction and, during summer, $4'$ in the north-south direction.

From one-dimensional observations of the two arrays, two-dimensional maps are computed using Earth rotation aperture synthesis (Alissandrakis et al., 1985). In the case of the two-dimensional maps, the resolution is slightly less than for the one-dimensional scans. For a declination of 23°, the resolution is, for example, $1.5'$ E-W by $4.2'$ N-S. An angular gap in the coverage of the u-v plane renders necessary the "cleaning" of the maps (Högbom, 1974), in an attempt to free them from sidelobes.

All synthesis methods assume that the brightness distribution remains constant during the observing period. Intense bursts are removed from data before map computation. In the case of strong or moderate noise storm emission, maps cannot be computed because of the large variations in brightness temperature. On the other hand, sufficiently faint noise storm continua can be mapped without any problem. A second limitation of Earth rotation aperture synthesis, mostly in the winter, is the presence of atmospheric gravity waves producing apparent motion of the radio sun (Mercier 1996). To minimize ionospheric effects, data used here were obtained during summer.

The amplitude and phase calibration is done by observing celestial sources of known intensity distribution such as Cygnus A, since strong point sources are rare at 169 MHz. During the period under study, in 1984, observations were also done with the Nançay interferometer at 169 MHz, providing independent calibration. Comparison of the flux measured with the two Nançay instruments and other instruments has been discussed in paper I. Over the fifty Nançay daily observations at 169 MHz (with mean flux of 6.65 s.f.u.), the average difference between our measurements and the flux interpolated from other instruments was 0.03 s.f.u. with a standard deviation of 0.28 s.f.u. (about 5% of the mean flux). Taking into account this result, the accuracy of the brightness temperatures measured on a map is estimated to be about $\pm 10\%$.

3. Large scale structures of the radio corona

Maps of the Sun at 169 MHz were obtained from May to August 1984, in the declining phase of the solar cycle. During this period, which is somewhat similar to the Skylab period one cycle earlier in 1973, the north and south coronal holes sometimes crossed the equator and were extended and rather stable features of the corona. The fifty daily maps obtained at 169 MHz correspond to Carrington rotations 1748 to 1752. For rotations 1750 and 1751 which are the best covered, ten days could not be mapped due to high noise storm activity.

At meter wavelengths the corona is seen at the same time on the disk and beyond the limb. Its brightness distribution shows, except in polar regions, a flat top, a rapid drop near the half maximum level (located near the optical limb) and an extended low brightness emission outside the disk. The characteristics of the quiet Sun at meter wavelengths vary with the solar cycle. The brightness temperature at the center of the disk is about $5\,10^5$ K during minimum (Lantos et al., 1992) and about $8\,10^5$ K during the maximum (Alissandrakis et al., 1985) when the contribution of the coronal plateau (see later) is removed. At the same time, the extent of the corona changes during the solar cycle. But, in addition, one notes very large variations of the shape of the quiet sun from day to day, due to the presence of dense structures beyond the limb. An example of strong asymmetry in the East-West as well as in the North-South direction is shown in the map of Fig. 2.

Fig. 1a shows a map obtained with the Nançay Radioheliograph on July 15 1984, at 169 MHz. The first contour outside the disk corresponds to a brightness temperature of 200 000 K. The contour interval is 50 000 K inside the disk and 100 000 K outside the disk. The maximum brightness temperature, in the western emission source, is $8.4\,10^5$ K.

The quiet sun at meter wavelengths has three distinct large scale components: coronal holes, the coronal plateau and a background. A coronal hole observed in the northern hemisphere in the HeI 1083 nm line (Solar Geophysical Data, 1984) is seen on the radio map as a depression in brightness (hatched contours), as is the case from centimeter to meter wavelengths (see for example Fürst & Hirth, 1975, Dulk & Sheridan, 1974). Note that, at decameter wavelengths, coronal holes are sometimes seen in emission (Dulk et al., 1977, Lantos et al., 1987). The lowest brightness temperature at the center of the coronal hole is about 600 000 K. The comparison of the location and shape of the present coronal hole on He and radio synoptic maps shows reasonable agreement (see Fig. 5b of paper I) but, on the daily map shown here, where the coronal hole is not close to the meridian, the difference between the shape of Helium and radio hole is important and even the overall orientation differs. The distortion of the radio image of the hole far from the meridian is probably due to radiative transfer and refraction effects. Nevertheless, new information can be obtained from radio observations, the radio and the He lines (or the X-rays) being sensitive to different parameters of the solar atmosphere. The use of four frequencies at radio wavelengths, available now with more recent version of the Radioheliograph, will help in discussing the possible causes of discrepancy between observations obtained in different wavelength ranges.

The coronal plateau has been described by Lantos et al. (1992) during a period of cycle minimum. It is defined more precisely on daily maps, even though synoptic maps show very well the overall structure (Lantos & Alissandrakis, 1996) and its

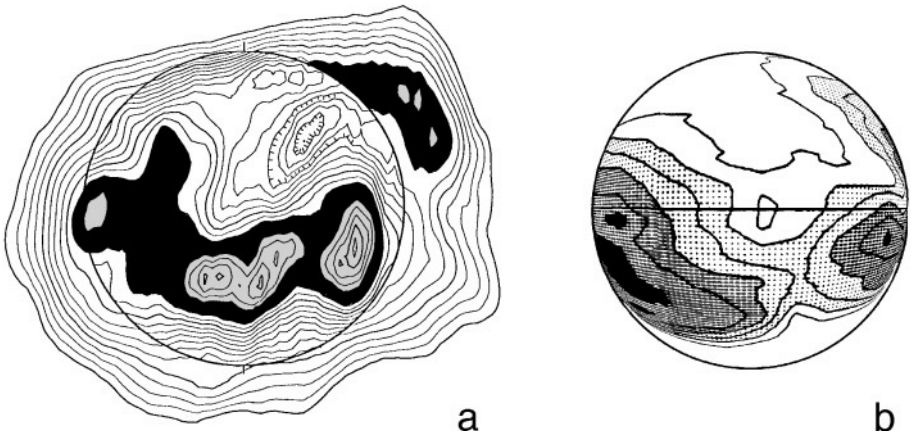

Fig. 1. a Map of the sun at 169 MHz, obtained on July 15, 1984 with the Nançay Radioheliograph. The black region is the coronal plateau (the radio counterpart of the coronal plasma sheet). A coronal hole is indicated by the hatched contour. **b** The corresponding K-corona synoptic map, on spherical projection

close relationship with the coronal plasma sheet observed with K-corona instruments. In Fig. 1 the coronal plateau is drawn in black on the disk. This feature has been defined on daily maps as a region forming a belt around the sun and surrounding almost all local emission sources (Lantos et al., 1992, Lantos & Alissandrakis, 1992a). To get a continuity over the sun of this new quiet sun component, a range of brightness temperatures of $5\,10^4$ K to 10^5 K, below the lowest source contour, has to be taken. In Fig. 1, the brightness temperature of the coronal plateau is $6.75\,10^5 \pm 2.5\,10^4$ K. On daily maps one notes also a center-to-limb effect on the coronal plateau which becomes less bright close to the limb (here on the western side), except if a local source exists on the limb (as on the eastern side here). Fig. 2 shows even more strongly this center-to-limb effect.

Fig. 1b provides a comparison of the shape and location of the coronal plateau with the corresponding part of the K-corona synoptic map (Fisher et al., 1985), projected on a sphere. The comparison reinforces the identification of the coronal plateau with the coronal plasma sheet (i.e. with the streamer belt), seen beyond the limb in the optical range. Previous work on the same subject (Lantos et al., 1992) referred to a period of cycle minimum. At that time the coronal plasma sheet was almost equatorial, with only a few excursions; an alternative explanation of the coronal plateau emission could be in terms of an axisymmetric model of the coronal density, like the one of Saito (1970). The present data, obtained during the declining phase of the solar cycle when the coronal plasma sheet strongly oscillates from one hemisphere to the other, renders more obvious the identification of the coronal plateau with the plasma sheet observed in the K-corona. Note also on Fig. 1a that the radio counterpart of the coronal plasma sheet is not only seen on the disk, but also beyond the North-West limb (emission plotted in black). It should be mentioned that such a local emission is exceptional for the quiet sun beyond the limb. Its maximum brightness temperature is about $5.5\,10^5$ K at $1.3\,R_\odot$.

Hakamada (1987), with a current free extrapolation of the photospheric magnetic field, showed that a high altitude loop system exists which overrides the principal neutral line. The origin of the diffuse emission of the coronal plateau is presumably due to this loop system, with a possible contribution of magnetic field loops connecting active regions to surrounding

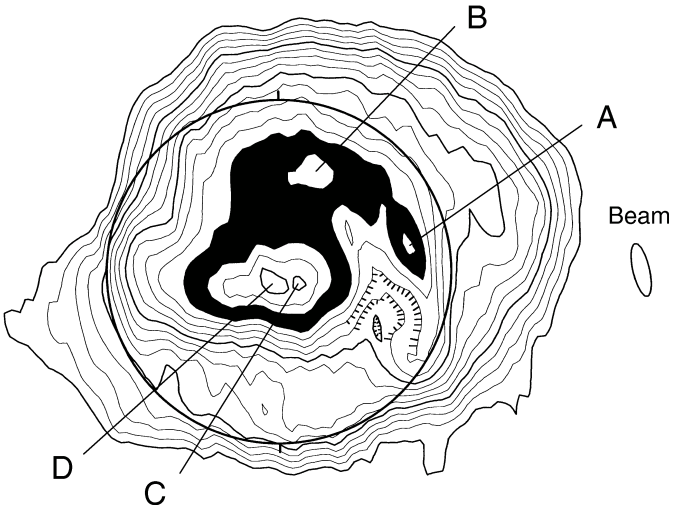

Fig. 2. 169 MHz map of the sun on June 9, 1984. The coronal plateau is filled in black.A coronal hole is indicated by the hatched contour. Emission sources A, B, C and D are discussed in the text.

quiet areas. This interpretation is reinforced by the observation of an isolated streamer, 100 000 K brighter at 164 MHz than the surrounding quiet sun (Lantos & Alissandrakis, 1992b). In this case, by comparing the location of 164 MHz source with two nearby 435 MHz sources, the streamer emission was attributed to a loop system. Note that alternatively a streamer model (Chiuderi-Drago, 1994) attributes the origin of brightness enhancement to the helmet part of the streamer. Nevertheless Lantos (1999) has given some arguments which reinforce the first explanation, including the presence of center-to-limb effects.

4. Medium scale structures

The local sources within the coronal plateau on Fig. 1 are of different nature. The one close to the west limb is a non-thermal noise storm continuum, while the others are classified as thermal sources, as will be discussed in detail in the following sections of this article.

Fig. 2 shows a map obtained on June 9, 1984. The resolution is $1.5'$ in East-West by $4.2'$ in North-South. Contours are

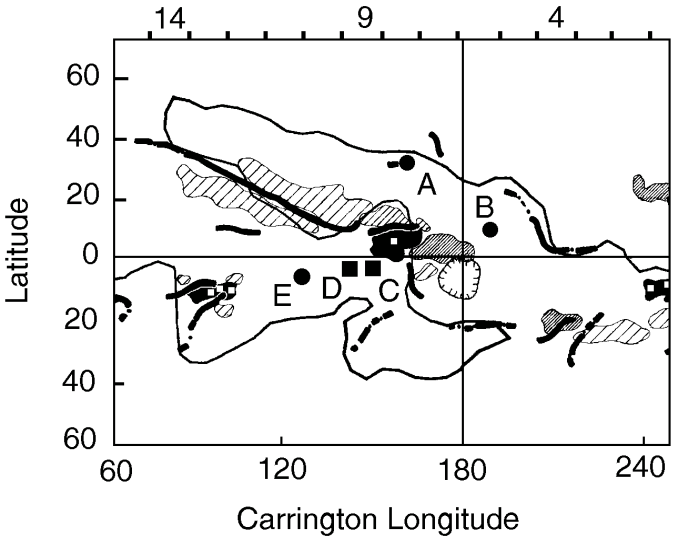

Fig. 3. A part of the Meudon synoptic chart for Carrington rotation 1749. Neutral lines, filaments and faculae are indicated. Sunspots are indicated with small white squares. A to E mark the positions of 169 MHz sources. Squares indicate sources close to sunspots and circles indicate the others. A coronal hole is shown by hatched contour.

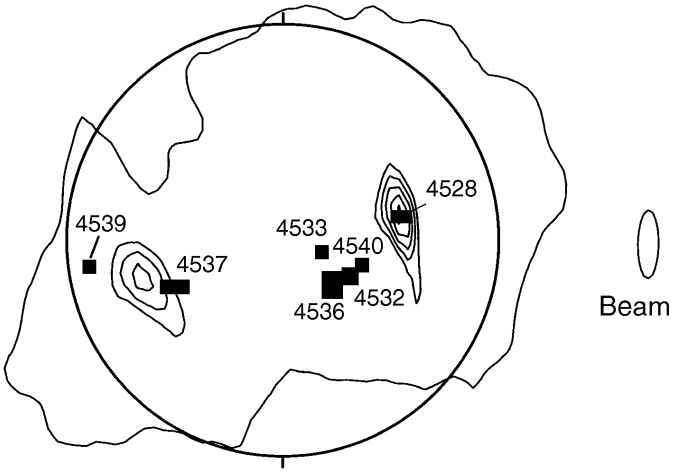

Fig. 4. Sources associated with noise storms on July 10, 1984. The outer contour corresponds to a brightness temperature of $5\,10^5$ K. The noise storm locations are indicated with the other contours. Boulder active region numbers are given.

separated by $5\,10^4$ K in brightness temperature and the lowest level is at $2\,10^5$ K. Four emission sources are seen on this map, surrounded by the coronal plateau. The coronal plateau is filled in black and corresponds to $8.5\,10^5 \pm 5\,10^4$ K. Outside the photospheric disk the brightness of the radio corona is very asymmetric, with a bright western limb, as already mentioned. The low brightness on the north-east limb indicates the presence of a coronal hole.

Fig. 3 shows a part of the Meudon synoptic chart (Martres & Zlicaric, 1986) for Carrington rotation 1749; Hα filaments are drawn in black and chromospheric faculae are hatched according to their brightness, except when sunspots (white squares) are present; they are filled in black in this case. A coronal hole, taken from Boulder synoptic chart (Solar Geophysical Data, 1984) is shown as a hatched contour. This coronal hole is seen as a brightness temperature depression on Fig. 2, south of the equator in the western hemisphere. The lower brightness temperature of the coronal hole is about 600 000 K, as in the previous example of coronal hole.

The radio sources of Fig. 2 have been placed on the synoptic map as well as a source, labelled E, observed only on June 13. All sources shown here are in the surroundings of faculae. Nevertheless subsequent discussion will enable us to give more precise identifications. The sources labelled B and E are in the middle between neutral lines and facular borders. They are part of the basic sample of thermal sources related to faculae. The twin sources C and D are close to the nearby sunspot and thus their thermal/non thermal nature is ambiguous. Nevertheless, the discussion of Sect. 5.1 gives arguments for their thermal origin. The source labelled A is located very close to a neutral line, as shown by the presence of an Hα filament. Discussion in the same section shows that this source is very likely related to an isolated streamer.

4.1. Faint noise storms

Using observations with the Culgoora radioheliograph at 80 MHz, Sheridan (1970) gave an example of a rather stable, non-thermal source seen at the same location as type I bursts. He also mentioned similar sources bulging above the limb. With the Nançay Radioheliograph, Alissandrakis et al. (1985), at 169 MHz, also observed faint noise storm continua identified by the presence of a few Type I bursts. Like the classical noise storms (Lesqueren, 1963), these emission sources are close to spotted active regions, but are generally not located above them. Their location and brightness temperature are less stable than for other sources. In addition, they are often narrower and brighter than thermal sources (see Sect. 5.1) and are visible above the limb, contrary to most thermal sources.

During the period under study, we observed 16 unambiguous noise storm continua. Fig. 4 shows two examples on the map of July 10, 1984. For readability, only one isophote of the quiet sun is drawn, corresponding to a brightness temperature of $5\,10^5$ K. One noise storm source is near the active region 4537 in the east; it has a peak brightness temperature of $1.2\,10^6$ K and an apparent half-power diameter of $4.6'$ in the east-west direction. The second is above the active region 4528, has a brightness temperature of $1.4\,10^6$ K and an apparent diameter of $2.1'$. All the observed noise storm continua have brightness temperatures above $8\,10^5$ K, when they are observed on the disk. The strongest has a brightness temperature of about $3.8\,10^6$ K. As only very few Type I bursts are detected (see Alissandrakis et al., 1985), they have no effect on the measured brightness temperature.

Fig. 5 shows a noise storm continuum observed above the limb on the map of June 20, 1984. The corresponding active region (Boulder number 4509) is located just behind the

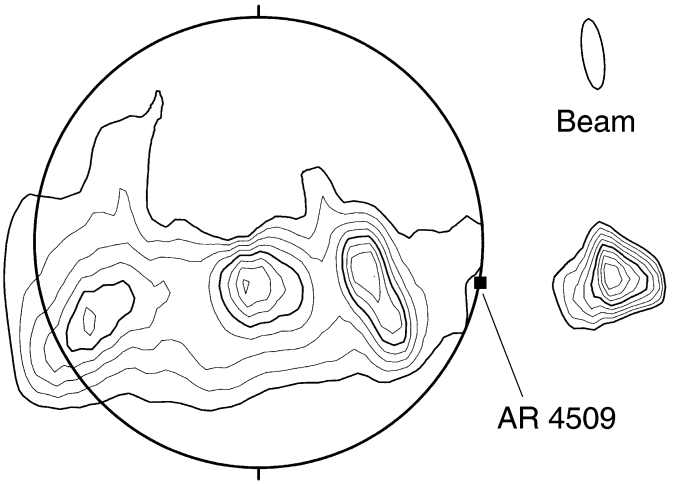

Fig. 5. A noise storm continuum above the West limb on June 20, 1984. The corresponding active region (Boulder number 4509) is indicated.

limb at 11° south latitude. The lowest isophote corresponds to 800 000 K and the isophote interval is 100 000 K. The maximum brightness temperature of the source is $1.6\,10^6$ K. The apparent distance of the source from the disk center is 1.58 $R_\odot$, corresponding to an apparent altitude of about $4\,10^5$ km. Assuming that the emission is at the 169 MHz plasma level, its density corresponds to 30 times the density of the Saito equatorial model during minimum (Saito, 1970). Note that, due to refraction of the rays in the corona, the apparent altitude provides only a minimum value of the true altitude.

On the disk, thirteen of the continua observed during the period under study, are within 10 synoptic map degrees of the nearest sunspot. Two are at about 15° and one is at 24°. Thus we shall retain the limit of 20° to discriminate between sources whose nature is ambiguous (inside this limit) and those presumably thermal in nature (outside this limit).

4.2. Relationship between radio sources and chromospheric faculae

A first point to be mentioned is that the thermal sources are outside faculae (23 out of 24 sources with distance from sunspots greater than 20°). The locations of the facula borders were taken from the Meudon synoptic charts, while the location of the sources were obtained from the average of their daily locations in Carrington coordinates. We assumed a height of 0.10 $R_\odot$ above the photosphere (we shall return later to the estimate of altitude). The beam of the instrument at 169 MHz corresponds, at the center of the disk, to 5° in the East-West and 15° in the North-South direction. We assumed that the sources observed from day to day were identical, if the distance between their centroids was smaller than 10° in Carrington longitude and latitude. Changes in the location of a source from day to day could be either intrinsic or only apparent, since refraction can indeed modify their apparent position.

To interpret the distribution of the observed distance between sources and facular borders, it is necessary to compare it with a random distribution, as was done for photospheric neutral lines and Hα filaments in paper I. The random draw must respect the latitude of the observed sources because of the important differences in latitude. It is furthermore necessary to treat each Carrington rotation separately, because of the evolution of faculae from one rotation to another. Thus we drew 400 groups of 23 sources, the only random variable being the Carrington longitude.

The results are shown in Fig. 6a. The bins of the histogram are 2° wide; black bars correspond to the observations, open bars to the random distribution. We can see that the number of observed sources becomes greater than that of the random distribution for a distance of 6°. A confidence criterion is defined for each distance class, as the fraction of draws with a smaller number of sources than the observed (see paper I). The criterion is given Fig. 6b. These results indicate that metric radio sources are related to faculae and that the closest significant distance from facular borders is from 4 to 8°.

On the basis on the configuration of the magnetic field we removed four sources from our sample. These were far from facular borders (between 22 and 35°) and, in addition, a neutral line intervened between them and the nearest facula, making their association with the facula impossible.

5. Study of thermal sources

5.1. Extension of the sample

So far we have considered as thermal only the sources that were far from sunspots. As pointed out in Sect. 4.1, noise storm continua have greater brightness and smaller diameter than thermal sources. Although each of these criteria alone is not sufficient to identify a source as thermal or noise storm, the relationship between them might help to identify some thermal sources which were not included in the sample because they were less than 20° from a sunspot.

Fig. 7 shows the diameter (full width at half maximum) of the sources as a function of their brightness above the background level. We chose the quiet sun level as the background rather than the coronal plateau, because the latter gave diameters sometimes smaller than the instrumental beam. The filled circles represent thermal sources located more than 20° away from sunspots and the filled squares correspond to sources identified as noise storm continua, in the manner described in Sect. 4.1. Note that in the figure the abscissa is restricted to $8\,10^5$ K, whereas two noise storm continua are above this limit (with respectively 1.5 and $3\,10^6$ K, with diameters of about 2′). The noise storms have a diameter of $4 \pm 2'$, except one which could be suspected to have multiple components.

The straight line is the linear regression line for the thermal sources (filled circles). It is reasonable to assume that all sources located above the regression line are thermal, even if they are not far from sunspots. Therefore, from the set of sources closer to 20° from sunspots, we retained as thermal those above the regression line. We were thus able to extend our sample from 47 sources identified on daily maps (corresponding to 19 distinct sources) to 60 daily thermal sources (27 distinct).

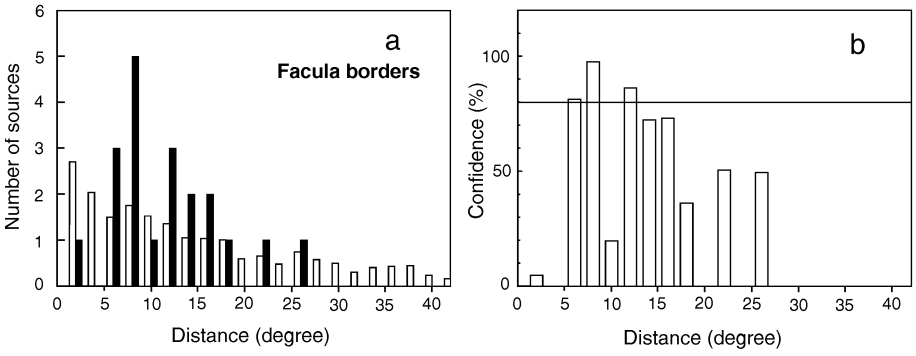

Fig. 6. a Distribution of the distance of sources from facular borders (black bars); open bars represent the distribution of a random draw. **b** The criterion of confidence (see text).

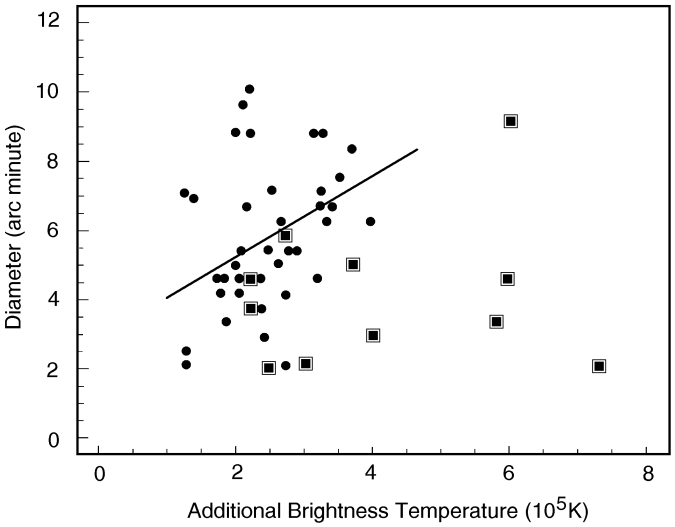

Fig. 7. Source diameter as a function of brightness. Filled circles are thermal sources and filled squares noise storm continua. The straight line is the regression for the thermal sources.

Nevertheless some of those sources are much closer to neutral lines than to facula borders (see explanations of Fig. 9b). The source labelled A in Figs. 2 and 3 is an example. Some of them are likely to be associated with loops of isolated coronal streamers (Lantos & Alissandrakis, 1992b). Thus they were removed from the sample of the thermal sources that might be unambiguously associated with faculae.

5.2. Characteristics of thermal sources associated with faculae

Fig. 8 gives histograms of characteristic parameters of the selected thermal sources. The distribution in longitude (Fig. 8a) is rather flat till about 30° and then drops; it is similar to the histogram in Fig. 3c of Lantos et al. (1992) for the minimum of the cycle. This effect was explained in terms of the occultation of the sources far from the central meridian, as a result of refraction. Indeed, thermal sources at meter wavelengths are rarely seen for more than four consecutive days. Fig. 8b, at the bottom left, gives the histogram of the latitude distribution. In addition to the center-to-limb effect, we have an asymmetry of the histogram in latitude.

Fig. 8c gives the distribution of the brightness temperature, measured above the quiet sun background. It is close to a gaussian, with a mean value of $2.4\,10^5$ K and a standard deviation of $7.7\,10^4$ K. Finally, Fig. 8d gives the histogram of the E-W diameters; the gaussian fit gives a mean value of 6.2′ with a standard deviation of 1.9′. Thus the sources are broader than the lobe of the instrument (which is about 1.5′ in the E-W direction).

5.3. Altitude of the thermal sources

Because of the short visibility of the thermal sources on the solar disk, the determination of the altitude of each source using its rotation rate is very difficult. Thus, assuming a rigid rotation, we shall consider all the sample together to derive a mean altitude. This hypothesis is justified by works done on the rotation of long lived CaII structures (Antonucci et al. 1977) as well as on rotation of K-corona structures (Fisher & Sime, 1984) and of X-ray emitting loops in the corona (Weber et al., 1994). For the coronal radio sources, the transformation of apparent location on the disk to heliographic coordinates requires the altitude of the sources as a parameter. Inversely, when the rotation rate is given, the mean altitude can be computed from the observed change of longitude at a given latitude from day to day.

We calculated that the best fit, corresponding to a synodic rotation rate of 13.25° per day (Antonucci 1977, Fisher & Sime, 1984), is found with an altitude of about 70 000 km above the photosphere (i.e. 1.10 $R_\odot$ from the Sun's center). With a synodic rotation rate of 12.1° per day (Weber et al., 1994), the altitude of thermal emission sources at 169 MHz would be 140 000 km (1.20 $R_\odot$ from the Sun's center). Because the meter wavelength sources are emitted at higher altitudes than the X-ray loops seen with Yohkoh SXT (which present a picture similar to the 410 MHz corona according to Lantos et al., 1995) and because meter wavelength quiet sun shows structures close to those observed with K-corona observations (paper II), the first value is probably the best. Nevertheless, since the standard deviation, even with this method, remains quite large, this must be considered as an estimate rather than as a precise measure. An altitude of 70 000 km for the critical density at 169 MHz (N_e=$3.5\,10^8$ cm^{-3}) corresponds to 2.2 times the equatorial Saito model of the quiet sun during the minimum of the solar cycle (Saito, 1970), which is a reasonable factor for the loops during the period of the cycle under study.

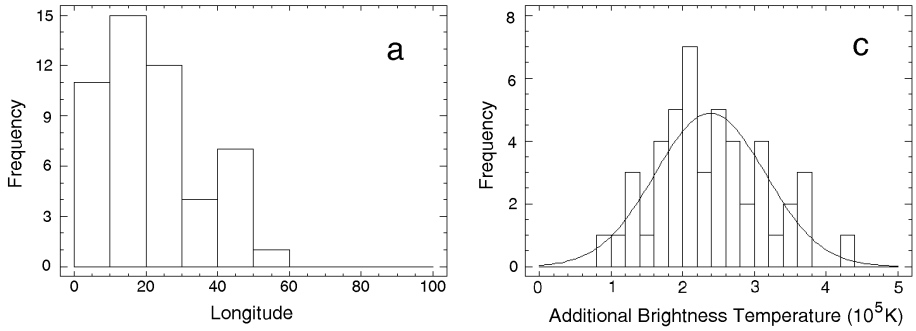

Fig. 8a–d. Distribution in longitude, latitude, brightness temperature and diameter of the selected thermal sources.

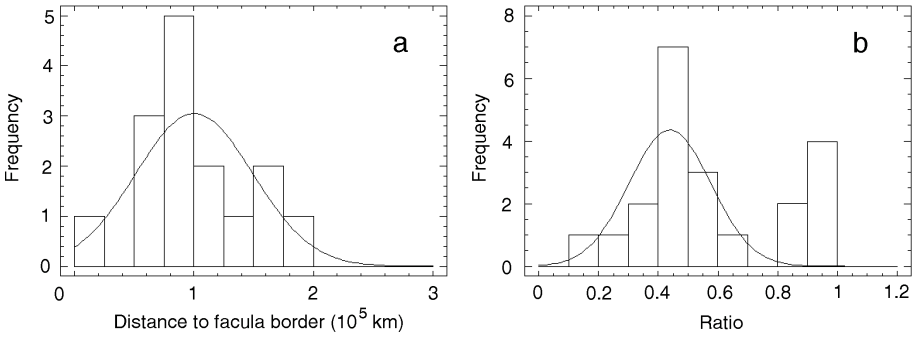

Fig. 9a and b. Histograms of the distance of thermal sources from facular borders **a** and the ratio between this distance and that from the nearest neutral line **b**. Abscissa is 0 for the facula border and 1 for the neutral line.

5.4. Model of thermal sources associated with faculae

As pointed out above, most of the thermal sources observed at 169 MHz are located outside active regions. Fig. 9a shows the histogram of the distance of these sources from facular borders. The mean distance is 100 000 km with a standard deviation of $4.9\,10^4$ km. On the other hand, as shown in paper I, a close relationship exists between the thermal sources and photospheric neutral lines outside active regions. The sources are thus mostly distributed between neutral lines and the border of the faculae, as illustrated in Fig. 3.

Fig. 9b gives the histogram of the distance of the sources from the closest facular border, divided by their distance to the closest neutral line. A source at the origin of the diagram would be on a facular border and a source at unity would be above a neutral line. The distribution of the ratio is close to gaussian, with a mean value of 0.44 and a standard deviation of 0.14. Despite the limited number of sources, this histogram suggests that sources with ratio beyond 0.8 are members of a different class, in which the emission is not necessarily related to the presence of faculae. If we consider this set of sources, as well as the few sources previously removed from the sample (see the last paragraph of Sect. 4.2), half of them are close to an Hα filament. In addition, almost all of the sources are in regions of enhanced density at $1.7\,R_\odot$ on the K-corona synoptic maps taken from Fisher et al. (1985) Thus an identification, at least for some of these sources, with loops at the base of an isolated coronal streamers seems likely. It should be recalled that those sources, even at high latitudes, are located in the coronal plateau and thus they are candidates to contribute to the streamer belt.

The above results suggest a model of the geometry of the thermal emission sources at meter wavelengths shown in Fig. 10. The loop system drawn at the right connects a facula with a region of opposite polarity beyond a photospheric neutral line. This medium scale loop system is sufficiently high to have the relatively low densities needed for metric wavelength emission. On the contrary, the smaller scale loop system shown on the left of the figure, which interconnects the two opposite polarities inside the facula, has much less chance to emit at meter wavelength because its density would be too high. We remind the reader that spotted active regions have no thermal counterpart at meter wavelengths for the same reason (see paper II). The higher density small scale loop is expected to emit at decime-

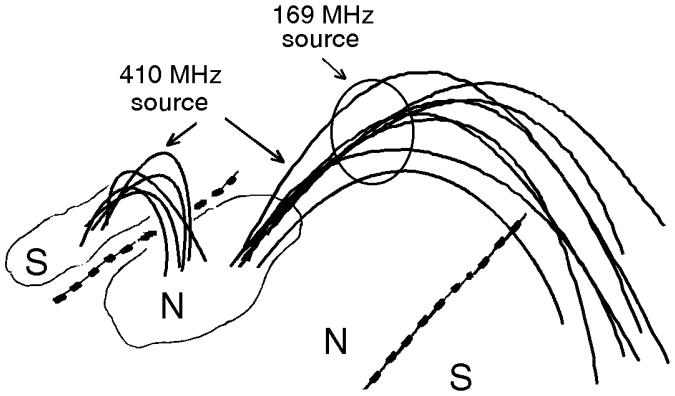

Fig. 10. Geometry of thermal decimetric and metric sources with respect to a facula. Neutral lines inside and outside the facula are drawn and assumed magnetic polarities are indicated.

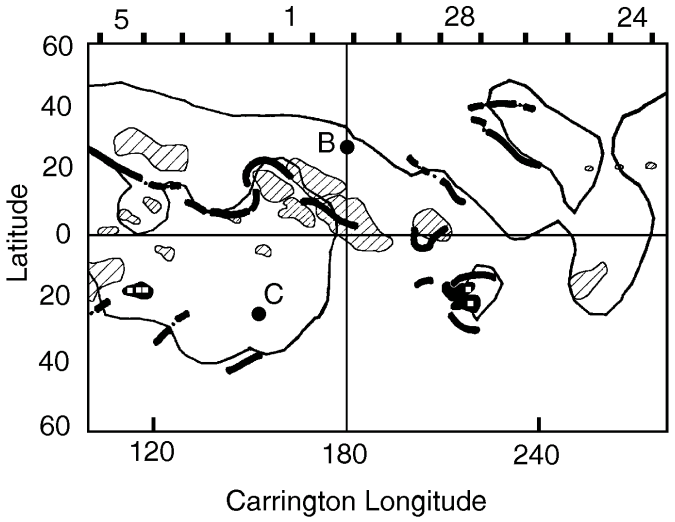

Fig. 11. Part of the Meudon synoptic chart for Carrington rotation 1751 for comparison with Fig. 3. The positions of two metric sources B and C are marked with black circles. Drawing conventions are the same as in Fig. 3.

ter wavelengths, e.g. at 410 MHz, (critical plasma density of $2.1\,10^9$ cm^{-3}).

Two additional observations reinforce the model proposed here. Fig. 11 shows the central part of the Meudon synoptic chart for Carrington rotation 1751 (Martres & Zlicaric, 1986). The positions of radio emissions observed at meter wavelengths are also shown on the map. Two of the sources plotted on Fig. 3 (Carrington rotation 1749) are still present after two solar rotations, the sources labelled B and C (or D). A comparison of this figure with Fig. 3 shows the displacement of the radio sources to the North for source B and to the South for source C (or D). While the first one may be related to the extension of the facula to the North, along the central meridian, the second suggests a close relationship with the extension of the neutral line to the South. During Carrington rotation 1750, both sources were at intermediate locations.

Fig. 12 shows, for a different period (during the 1986 solar minimum when multifrequency observations were available, see Lantos et al., 1992), the locations of radio sources observed at three frequencies: 410 MHz (on the left), 327 MHz (at the center) and 164 MHz (on the right). From higher to lower frequency the emissions tend to move away from the center of the facula, as predicted by the model of Fig. 10, since lower frequency corresponds to lower loop density.

6. Discussion and conclusions

In the present work we identified a metric source component associated to, but not located above faculae. We also presented some meter wavelength radio streamer candidates. Over a total sample of about fifteen distinct sources, these identifications indicate that, during this period of the solar cycle (two year before the minimum), 40% of the sources are related to faculae and are thermal in nature. Their geometry was explained in terms of the model discussed in Sect. 5.4. In addition, another 22% of the sources are also thermal and apparently not related to faculae. Most of them override photospheric neutral lines and they could be loops at the base of isolated coronal streamers. Nevertheless, according to K-corona observers (e.g. Sime & McCabe 1990), it is necessary to use high altitude data (sun distances above 1.7 $R_\odot$), to separate streamers from other loop systems (called "bright points" by Sime and McCabe). Non-thermal sources (faint noise storm continua) during this period represent at least 13% of the sources, while the nature (thermal or non-thermal) of about 25% of the sources was not identified. Observations with polarization measurements, available with the last version of the Nançay Radioheliograph (Kerdraon & Delouis, 1997), will facilitate the identification of the faint noise storms.

The identification of the sources, and in particular streamers on the disk, is important not only for modelling purposes, but also in terms of the relationship between coronal structures and solar wind regimes. The detection on the disk of the coronal plasma sheet (the coronal plateau) will also be useful for such studies because the longitudinal resolution is much better with radio observations than with K-corona or coronal line observations beyond the limb.

The altitude of the sources is an important parameter for the interpretation of the emissions in terms of models. As mentioned above, measurements of the altitudes at meter wavelengths are difficult, because of the short visibility of the thermal sources on the solar disk and also because of their sizes. The average altitude found here, of about 1.1 $R_\odot$, must be considered as a rough estimate. A preliminary study (Lantos et al., 1995) showed that 410 MHz maps are the ones that resemble most to Yohkoh images; therefore, it is likely that meter radio emission on the solar disk originates in loops at altitudes higher than the X-rays. This is one of the important reasons why the quiet sun at meter and decameter wavelengths deserves further studies, in particular in the frame of the Solar-Terrestrial Physics and Space Weather projects as pointed out by Lantos (1999). Indeed Simon & Legrand (1993) have shown that 90% of the time

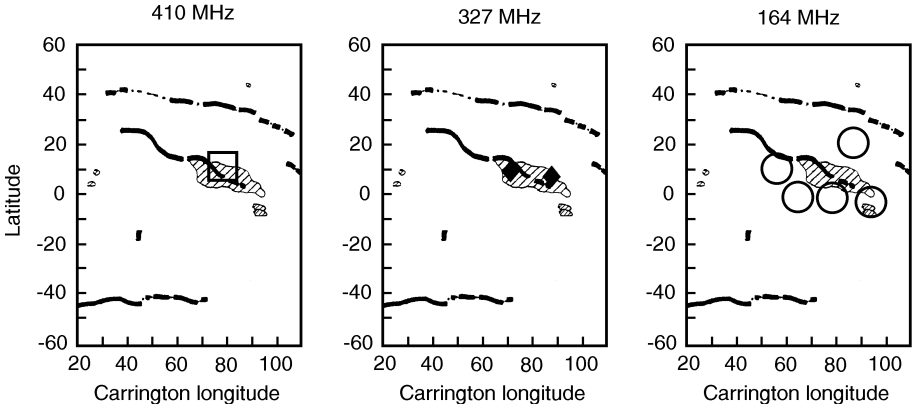

Fig. 12. Location of radio sources close to a facula at three frequencies, on Meudon synoptic charts for a period during the 1986 minimum. On the left side, the source at 410 MHz is marked with an open square. At 327 MHz (in the middle) the radio sources are indicated with black diamonds. On the right side, sources at 169 MHz are marked with open circles.

the geomagnetic activity is dominated by the effects of coronal structures rather than by flares and CME's.

References

Alissandrakis C. E., Lantos P., 1996, Solar Phys., 165, 61 (paper I).

Alissandrakis C. E., Lantos P., Nicolaidis E., 1985, Solar Phys., 97, 267.

Antonucci E., Azzarelli L., Casalini P. and Cerri S., 1977, Solar Phys., 53, 519

Chiuderi-Drago F., 1994, in Mass Supply and Flows in the Solar Corona, (B. Fleck, G. Noci and G. Poletto eds), Kluwer Academic Publishers.

Dulk G.A., Sheridan K.V., 1974, Solar Phys., 36, 191.

Dulk G.A., Sheridan K.V., Smerd S.F., Withbroe G.L., 1977, Solar Phys., 52, 349.

Fisher R. and Sime D.G., 1984, ApJ 287, 959

Fisher R. R., Garcia, C., Lundin, E., Seagraves, P., Sime D. G. and Rock, K.: 1985, NCAR Technical Note TN-246, High Altitude Observatory, NCAR, Boulder, USA.

Fürst E., Hirth W., 1975, Solar Phys. 42, 157

Hakamada K., 1987, J. Geophys. Res., 92, A5, 4339–4348

Högbom J.A., 1974, Astron. Astrophys. Suppl. 15, 417.

Kerdraon A. and Delouis J.M., 1997, in Coronal Physics from Radio and Space Observations (G. Trottet ed.), Springer-Verlag, Berlin.

Lantos P., 1999, in Solar Physics with Radio Observations, Proceedings of Nobeyama Symposium 1998, NRO Reports.

Lantos P. and Alissandrakis C. E., 1992a, in Solar Wind Seven (E. Marsch and R. Schwenn eds.), Pergamon Press, Oxford

Lantos P. and Alissandrakis C. E., 1992b, Proceedings First SOHO Workshop, ESA SP 348.

Lantos, P., Alissandrakis, C.E. 1996, Solar Phys., 165, 83 (paper II).

Lantos P., Alissandrakis C. E. and Rigaud D., 1992, Solar Phys., 137, 225.

Lantos P., Alissandrakis C.E. and the Yohkoh Team, 1995, Advance in Space Research, 17, 261

Lantos P. and Alissandrakis C. E., Gergely T., Kundu M., 1987, Solar Phys., 112, 325.

Lesqueren A. M., 1963, Ann. d' Astrophys., 26, 97.

Martres M.J. and Zlicaric G.: 1986, Cartes Synoptiques de la Chromosphère Solaire, vol VI, fascicule 6, Observatoire de Paris.

Mercier C. 1996, Ann. Geophysicae, 14, 42

Radioheliograph group, 1983 Solar Phys., 88, 383

Saito K., 1970, Ann. Tokyo Astron. Obs XII, 53.

Schmahl E.J., Gopalswamy N. and Kundu M.R., 1994, Solar Phys., 150, 325.

Sheridan K.V., 1970, Proc. ASA, 1, 304.

Sime D.G. and McCabe M.K., 1990, Solar Phys., 126, 267.

Simon P. and Legrand J.P., 1993, in Solar Terrestrial Prediction Workshop-IV (J. Hruska, M.A. Shea, D.F. Smart & G. Heckman eds.), NOAA and AFGL, USA.

Solar Geophysical Data (H.Coffey ed.), 1984, NGDC, NOAA, Boulder

Weber M., Acton L.W. and Alexander D., 1994, in Solar Dynamic Phenomena and Solar Wind Consequences, SP 373, p 405.